ACS OMEGA

http://pubs.acs.org/journal/acsodf

Article

Role of Intrinsic Defects in Enhancing the Photoabsorption Capability of $CuZn_2AlSe_4$

M. V. Jyothirmai and Ranjit Thapa*

Cite This: *ACS Omega* 2022, 7, 31098−31105

Read Online

ACCESS | Metrics & More | Article Recommendations | Supporting Information

ABSTRACT: As a promising candidate for low-cost and eco-friendly thin-film photovoltaics, the emerging quaternary chalcogenide based solar cells have experienced rapid advances over the past decade. Here, we propose quaternary semiconducting chalcogenides $CuZn_2AlSe_4$ (CZASe) through cross-substitutions (cation mutations). The nonexistence of imaginary modes in the entire Brillouin zone of CZASe represents the inherent dynamic stability of the system. The electronic, optical, and defect properties of stannite CZASe quaternary semiconducting material was systematically investigated using density functional theory calculations. We have found that the chemical-potential control is very important for growing good-quality crystals and also to avoid secondary-phase formations such as ZnSe, Al_2ZnSe_4, and Cu_3Se_2. The observed p-type conductivity is mainly due to antisite defect Cu_{Zn}, which has the lowest formation energy with a relatively deeper acceptor level than that of the Cu vacant site (V_{Cu}). The electronic band structures of vacancies and antisite defects by means of hybrid functional calculations show energy band shifting and energy band narrowing or broadening, which eventually tunes the optical band gap and improves the solar energy-conversion performance of semiconducting CZASe. Our results suggest that the stannite CZASe quaternary chalcogenides could be promising candidates for the efficient earth-abundant thin-film solar cells.

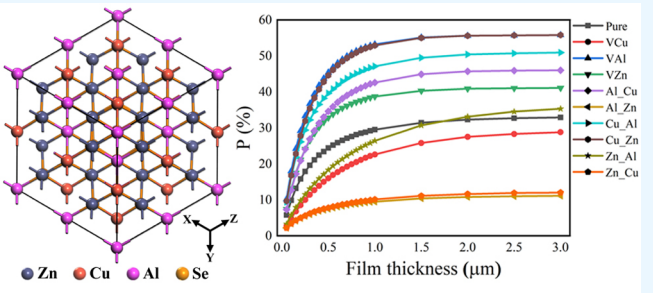

1. INTRODUCTION

First-generation solar cells, namely, single crystalline silicon-based solar technology, have dominated the photovoltaic industry by converting solar energy into electricity with a record efficiency of 25%.[1] However, a very low photon-to-electron conversion efficiency and relatively high expenditure of silicon solar cells has forced the search for new solutions.[2] Taking into consideration the advantages of cost-effectiveness, low toxicity, and earth abundant elements, the family of quaternary semiconducting chalcogenides, especially $Cu_2ZnSn(S/Se)_4$ (CZTS/Se), has been considered as the most useful materials for producing solar electricity.[3,4] The crystal structure and bandgap of CZTS/Se are similar to commercially available $Cu(In_xGa_{1-x})S/Se_2$ (CIGS) based solar cells,[5] despite the fact that the formation of a homogeneous and single-phase system is very difficult without the presence of secondary phases, which limits the absorption of solar spectrum and thereby reduces solar energy harvesting.[6] At this juncture, the quest for the design and synthesis of sustainable and affordable energy generation materials remains.[7−9]

To further enhance the efficiency and stability of semiconducting materials, new multicomponent quaternary chalcogenides can be designed by a series of cross-substitutions.[10,11] Using this structural and chemical freedom approach, various quaternary chalcogenides $I−II_2−III−VI_4$ (I = Cu, Ag; II = Zn, Cd; III = Si, Ge, Sn; and VI = S, Se, Te) were designed by cation mutations between binary II−VI and ternary $I−III−VI_2$ compounds (see Figure 1a), including $Cu_2FeSn(S/Se)_4$,[12] Cu_2BaSnS_4,[13] $Ag_2ZnSn(S/Se)_4$,[14] and $CuFe_2InSe_4$,[15] to improve the power conversion efficiency of absorber materials. Table S1 represents the electrical performance parameters of recently developed multicomponent quaternary semiconductors. It is clearly exemplified that the modification of the chemical structure with various elements improves the performance of the absorber materials. For instance, the Cu_2ZnGeS_4 system exhibits power conversion efficiency (PCE) of 5.5%, while the replacement of Zn with Cd in Cu_2CdGeS_4 material further improved the PCE to 7.67%. Despite this exponential improvement, the presence of multiple elements in quaternary chalcogenides makes it challenging to design single-crystal samples with good quality. Typically, such nonstoichiometry represents the high population of intrinsic defects, and their equilibrium concentration is determined by their electronic chemical potential as well as the formation energy (growth conditions). These defects can act as recombination centers due to deep states in the

Received: May 24, 2022
Accepted: July 20, 2022
Published: August 24, 2022

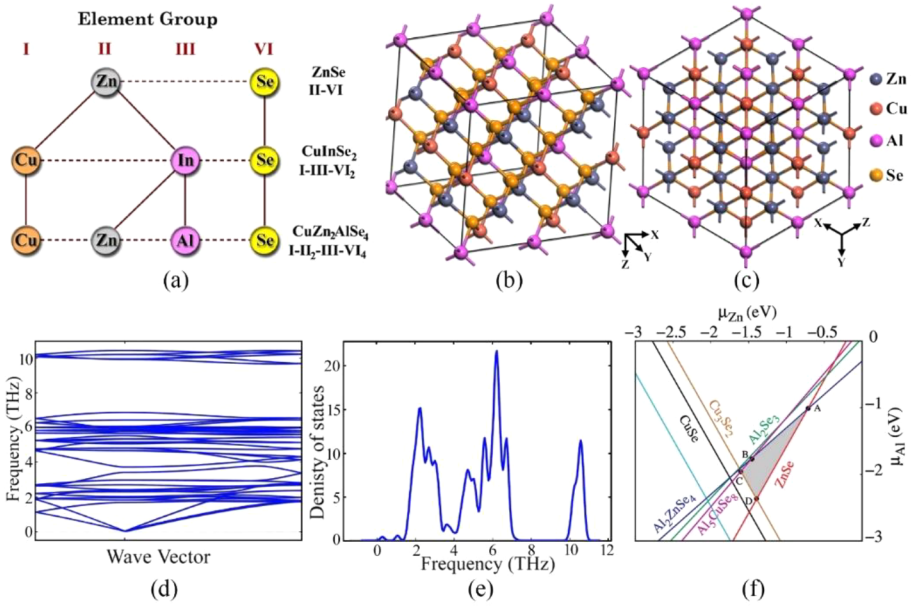

Figure 1. (a) Correlation between binary, ternary, and quaternary chalcogenides to module CZASe, beginning from II−VI parent material. (b,c) Crystal structure of CZASe along two different crystallographic directions. (d,e) Calculated phonon dispersion and phonon density of states of CZASe, (f) the 2D stability diagram of CZASe (for μ_{Cu} = 0 eV).

electronic band gap. Nagoya et al. reported the formation energies of vacancies (V_{Cu} and V_{Zn}) and antisite defects (Cu_{Zn}, Zn_{Cu}, Cu_{Zn}, and Zn_{Sn}) and found that the Cu_{Zn} antisite as most stable defect.[16] The clear understanding of the concentration of lattice defects, such as vacancies and antisites, are essential for elucidating the compositional reliance of the photovoltaic efficiency.

Theoretical and experimental work related to cross-substituted quaternary systems is quite limited, and very little work has been reported on $CuZn_2AlS_4$ (CZAS). The stannite phase $CuZn_2AlS_4$ (CZAS) is an interesting material having a direct band gap (1.61 eV) with a suitable position of valence (5.4 eV) and conduction band (3.8 eV) and a relatively high absorption coefficient ($\geq 10^5$ cm^{-1}).[17] Recently, Ghosh and co-workers[11,18] have synthesized $CuZn_2AS_4$ and Cu_2ZnAS_{4-x} (A = Al, Ga, In) semiconductors in which stannite phase is found to be more stable than zinc blende-, orthorhombic-, wurtzite-, and kesterite-type structures. Their results highlight the importance of low-cost absorber photovoltaic materials in solar energy applications due to their direct band gap (1.20−1.72 eV) and high optical absorption ($>10^4$ cm^{-1}). Subsequently, Yalcin[19] studied the ground-state properties of $CuZn_2AS_4$ (CZAS) (A = Al, Ga and In) nanocrystals using hybrid functional calculations. Recently, Wencong et al.[20] explored the phase stability for a series of quaternary chalcogenides with $I-II_2-III-VI_4$ chemical composition and found that the $CuZn_2AlSe_4$ (CZASe) structure is energetically stable in the stannite phase. This unexplored semiconducting chalcogenide CZASe can be modified by inducing defects that will allow relatively complex electronic and optical properties, which might bring further improvements in their use as solar harvesting materials.

Here, the formation-energy and the transition-energy levels were systematically investigated for a series of vacancies and antisite defects of quaternary chalcogenide $CuZn_2AlSe_4$ (CZASe) using first-principles calculations. The electronic band structure of defect-induced CZASe show energy band shifting and energy band narrowing or broadening. The absorption spectra demonstrate the significance of defects by introducing low energy excitations in the visible-light region. Since the knowledge of current density and upper limit of the theoretical power conversion efficiency is essential for the design and development of solar harvesting material, the corresponding values are also reported and the results highlight the importance of vacancies and antisite defects.

2. COMPUTATIONAL DETAILS

All electronic structure calculations for the designed CZASe material were performed under periodic boundary conditions using density functional theory via Vienna Ab initio Simulation Package (VASP)[21] within the framework of pseudopotential projector augmented-wave (PAW) method.[22] Geometry optimization was performed using the conjugate−gradient algorithm. The sampling of k-points in reciprocal space and the value of kinetic energy cutoff (size of the basis set) were chosen to be 7 × 7 × 7 and 450 eV, respectively. The generalized gradient approximation (GGA) developed by Perdew, Burke, and Ernzerhof was implemented to include the exchange-correlation potential.[23] The convergence criterion for self-consistent iterations and the maximal ionic Hellmann−Feynman forces were set to be 10^{-5} eV per atom and less than 0.01 eV $Å^{-1}$, respectively. During geometry optimization, the symmetry of crystals as well as the size of the unit cells were conserved to preserve the crystallinity of investigated chalcogenide structures. In order to obtain accurate electronic and optical properties, the Heyd Scuseria Ernzerhof 06 (HSE06)[24,25] hybrid functional that screens the Coulomb potential for the Hartree−Fock (HF) exchange is implemented using a 0.25 mining parameter. The dynamic dielectric function calculated through the HSE06 functional is used to evaluate the absorption spectrum. The power conversion efficiency and current density were measured according to our previously developed methodology.[26] In order to check the dynamical stability, phonon dispersion calculations were performed within the harmonic approxima-

https://doi.org/10.1021/acsomega.2c03223
ACS Omega 2022, 7, 31098−31105

tion through VASP using Phonopy code that utilizes the finite displacement method[27] via a supercell approach. To obtain accurate forces, the convergence criterion of the total energy was set to 10^{-10} au. The default PHONOPY displacement of 0.01 Å was employed for all the calculations. To correct possibly lost symmetries due to numerical inaccuracies, the obtained harmonic force constants were symmetrized with PHONOPY's internal subroutines.

In the present work, two types of defective systems were investigated: first, cation vacancies were created in the pure structure of CZASe by removing copper, zinc, and aluminum atoms and denoted as V_{Cu}, V_{Zn}, and V_{Al}, respectively. Second, the positions of zinc and copper (Zn_{Cu} and Cu_{Zn}), aluminum and copper (Al_{Cu} and Cu_{Al}), aluminum and zinc (Al_{Zn} and Zn_{Al}) were interchanged.

3. FORMATION ENERGY

The formation energy $\Delta H(\alpha,q)$ of a defect α in the charge state q and the corresponding charge transition level $\varepsilon(\alpha,q/q')$ calculations were performed using supercell approach with 64 atoms of the CZASe system

$$\Delta H(\alpha, q) = E(\alpha, q) - E(\text{host}) + \sum_I n_i(E_i + \mu_i) + q[\epsilon_{VBM}(\text{host}) + E_F] \quad (1)$$

where E(host) and $E(\alpha,q)$ represent the total energies of perfect and defect supercells, respectively. E_F is the Fermi energy, and ε_{VBM} is the energy of valence band maximum of the host material. n_i and μ_i are the number of atoms and atomic chemical potential of element i in CZASe. It should be noted that the concentration of "pure" CZASe is exclusively dependent on chemical potentials and is thermodynamically governed by several conditions. The defect transition-energy level $\varepsilon(\alpha,q/q')$ is the adiabatic transition energy between two defect charge states which is defined as the formation energy $\Delta H(\alpha,q)$ of the α defect with charge q equal to $\Delta H(\alpha,q')$ with a distinct charge q'. The complete description and implementation about the defect methodology can be found in refs 28 and 29.

4. RESULTS AND DISCUSSION

The quaternary chalcogenide $CuZn_2AlSe_4$ (CZASe) crystallizes in stannite structure (space group $I\bar{4}2m$) with lattice parameters a = 11.53 Å and c = 11.49 Å. Here, the cations Zn, Cu, and Al have +2, +1, and +3 oxidation states, while chalcogen anion Se possesses a −2 oxidation state. The weighted sum of the oxidation states in CZASe system is neutralized, which is a necessary condition for a material to be a semiconductor. Selenium atom is coordinated to two zinc, one copper, and one aluminum atom, forming a tetrahedron and thereby following the Lew's octet rule. Full geometry optimization was performed for the CZASe crystal structure (see Figure 1b,c), and the relaxed structural parameters are given in the Table 1.

4.1. Dynamical and Phase Stability. If a structure is a maximum on the potential-energy surface, then the frequencies of one or more vibrational motions will reduce, leading to dynamic instability of a crystal, while the minimum potential-energy structure has $\omega \geq 0$ (at the center of the Brillouin zone, the three acoustic modes have $\omega = 0$). Therefore, the vibrational spectra allow us to validate the stability of the material. The phonon dispersion spectrum and the phonon density of the states for CZASe structure are presented in Figure 1d,e. The band dispersion and phonon density of states does not show any imaginary frequencies in the entire Brillouin zone, indicating CZASe as a stable material.

Table 1. Calculated Lattice Parameters, Bond Distance, and Formation Energies of Pure and Defect Induced CZASe

	lattice parameters (Å)			
structure	a	c	bond distance (Å)	formation energy (eV)
pure	11.39	11.34	Cu 2.45 Zn 2.49 Al 2.43	
V_{Cu}	11.40	11.27		0.32
V_{Zn}	11.36	11.29		4.95
V_{Al}	11.35	11.34		7.43
Zn_{Cu}	11.44	11.38	2.51	2.16
Al_{Cu}	11.47	11.35	2.62	0.63
Cu_{Zn}	11.39	11.31	2.44	−0.48
Al_{Zn}	11.43	11.36	2.46	0.39
Cu_{Al}	11.37	11.33	2.42	2.57
Zn_{Al}	11.40	11.33	2.47	3.73

The prediction/synthesis of homogeneous quaternary semiconducting material without formation of unintentional secondary phases is the prime concern to achieve high-performance solar cells.[28−30] To obtain stable pristine CZASe, all possible secondary selenium phases formed by Cu, Zn, and Al atoms are taken into account, which may coexist at different growth conditions. Moreover, the formation of elemental solids should be avoided by considering atomic chemical potentials in CZASe smaller than that of corresponding elemental solids (i.e., $\Delta\mu_{Cu} < 0$, $\Delta\mu_{Zn} < 0$, $\Delta\mu_{Al} < 0$, $\Delta\mu_{Se} < 0$). Thus, the stable stoichiometric CZASe is obtained by maintaining the chemical potentials of constituent elements μ_i:

$$\Delta\mu_{Cu} + 2\Delta\mu_{Zn} + \Delta\mu_{Al} + 4\Delta\mu_{Se} = \Delta H_f(CuZn_2AlSe_4) = -6.7 \text{ eV}$$

Here, $\Delta H_f(CuZn_2AlSe_4)$ is the formation energy. Each chemical potential diagram corresponds to a plane cut at distinct values of $\Delta\mu_{Cu}$; the diagonal, height, and abscissa of every diagram are bounded by $\Delta H_f(CuZn_2AlSe_4/n\alpha(\alpha$ = Zn, Al and Se). The relations for $\Delta H_f(CuAlSe_4)$, $\Delta H_f(CuSe)$, $\Delta H_f(CuSe_2)$, $\Delta H_f(Cu_3Se_2)$, $\Delta H_f(ZnSe)$, $\Delta H_f(Al_2Se_3)$, $\Delta H_f(Al_2AnSe_4)$, and $\Delta H_f(Al_5CuSe_8)$ are given in the Supporting Information. These sets of conditions confine the stable CZASe chemical potential region in a polyhedron of $\Delta\mu_{Cu}$, $\Delta\mu_{Zn}$, and $\Delta\mu_{Al}$ three-dimensional space. The chemical potential-based stability diagram along with the other existing secondary phases are shown in Figure 1f, where the homogeneous and single-phase CZASe is clearly represented by gray regions ABCD. Depending upon growth environment, each line on the chemical potential diagram indicates the boundary of secondary phase that forms during the synthesis of CZASe. Moreover, the nonuniform control of chemical potential in the stable region of CZASe may lead to the formation of Cu_3Se_2, ZnSe, and Al_2ZnSe_4 phases, which indicates that these secondary compounds grow easily than other phases. Among three cations, μ_{Zn} shows relatively lower value (∼−0.7 eV) than μ_{Cu} (−0.55 eV < μ_{Cu} < 0 eV) and μ_{Al} (−1.01 eV < μ_{Al} < −2.5 eV) due to strong binding between Al and Zn and thus, the well-defined stable pristine CZASe is

https://doi.org/10.1021/acsomega.2c03223
ACS Omega 2022, 7, 31098−31105

limited only to the corresponding region. Any slight deviation of $\Delta\mu_\alpha$ (α = Zn, Al and Se) at $\Delta\mu_{Cu} = -0.35$ eV may force $CuZn_2AlSe_4$ to coexist with the secondary phases, which indicates P as one of the end points of the stable three-dimensional polyhedron (see Figure S1).

Therefore, the complex stable region at various (μ_{Zn}, μ_{Al}) planes demonstrate that the quality of the CZASe crystal growth is only possible by controlling the chemical-potential.

Typically, the formation energies are related to the formation ability of defects in the materials: The low formation energies usually affect the properties of host materials, while the high formation energies that exist in smaller amounts do not show much impact on the behavior of materials. As mentioned, the cation vacancies are created by removing copper, zinc, and aluminum atoms in the chalcogenide CZASe, represented by V_{Cu}, V_{Zn}, and V_{Al}. After creating Cu vacant site, the nearest Cu−Se bond lengths are compressed by about 0.039 Å when compared to its pure material. For V_{Zn} and V_{Al}, we could observe a decrease in the neighboring Zn−Se and Al−Se bond lengths of about 0.059 and 0.066 Å, respectively. Among three types of vacant sites in CZASe, the size mismatch of Al atom is higher such that the displacement of four nearest neighbor Se atoms around the V_{Al} vacant site is relatively large when compared with that of V_{Cu} and V_{Zn} vacant sites. On the other hand, Al in CZASe can replace Zn and Cu from their lattice sites and can create Al_{Cu} and Al_{Zn} antisite point defects. The Zn_{Cu}, Zn_{Al}, Cu_{Zn}, and Cu_{Al} antisite defects are also considered in CZASe, and the corresponding defect bond lengths are presented in Table 1. It should be noted that the Cu and Zn disorders possess similar chemical structures and form deep trap states, midgap states, shallow acceptor levels, and shallow donor level within the band gap.

The calculated formation energies as a function of the Fermi energy level for the defect charge states of CZASe is shown in Figure 2. Depending on defect formation energies and

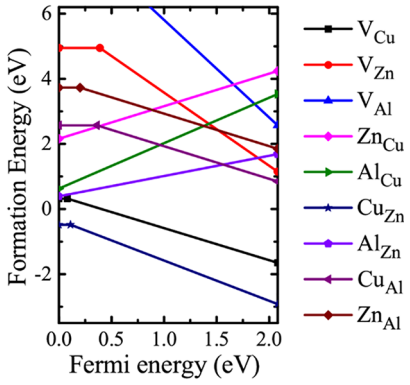

Figure 2. Calculated formation energies as a function of the Fermi energy level for the defect charge states. The negative (positive) slope of the line represents that the defect is an acceptor (donor). The defect is not ionized (or neutral) if the slope is equal to zero.

corresponding charge-state transition levels, the vacancies and antisite defects can form either donor or acceptor levels in CZASe. The acceptor defect Cu_{Zn} has the lowest formation energy when compared to other acceptor and donor defects, indicating acceptor Cu_{Zn} as a dominant defect in CZASe with intrinsic p-type semiconducting nature, similar to that of Cu_2ZnSnS_4. However, Cu vacancy (V_{Cu}) is the dominant p-type acceptor in ideal chalcopyrite $CuInSe_2$. The major variation between $CuInSe_2$ and $CuZn_2AlSe_4$ is that the huge difference between In and Cu in ternary $CuInSe_2$ forces the antisite defect Cu_{In} to possess higher formation energy than Cu vacancy (V_{Cu}), while the three types of cations in quaternary compounds give rise to more antisite defects due to the small valence difference between Cu and Zn, making the Cu_{Zn} antisite to have lower formation energy compared to that of V_{Cu}. Further, the formation energies of acceptors V_{Al} and V_{Zn} are much higher than the other defects.

The calculated charge-state transition levels for all of the studied vacancies and antisite defects in CZASe are shown in Figure 3. Among all studied defects, V_{Cu} (0/−) behaves like

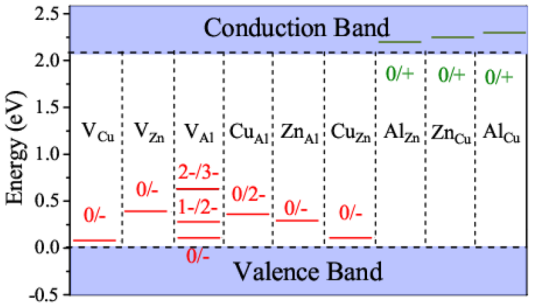

Figure 3. Calculated charge-state transition energy levels of vacancies and antisite defects in the band gap of CZASe.

shallow acceptor level just ∼0.11 eV above the VBM, which is beneficial to enhance the p-type behavior of the CZASe material. The antibonding coupling between the high-lying Se 4p orbitals and Cu 3d orbitals is responsible for th eshallow nature of V_{Cu}, which is similar to other semiconducting Cu-based absorbers like CZTS and CIGSe.[31,32] The calculated acceptor transition energy level for V_{Zn} (0/2−) is located at 0.39 eV above the VBM, whereas the transitions (0/1−), (1−/2−), and (2−/3−) of V_{Al} are observed at 0.11, 0.28, and 0.63 eV, respectively. The antisite acceptor defects Cu_{Al}, Cu_{Zn}, and Zn_{Al} has transitions (0/2−), (0/−), and (0/−) at 0.36, 0.18, and 0.2 eV above the VBM, respectively, while the charge-state transitions (0/+) for all of the antisite donor defects Al_{Cu}, Al_{Zn}, and Zn_{Cu} are located outside the bandgap region.

4.2. Electronic Properties. The open-circuit voltage defines the device performance and mainly depends on the band gap of absorber materials. Typically, the standard DFT functionals (i.e., LDA and GGA) has a limitation in predicting the correct band gap of semiconducting materials. To overcome this problem, the electronic band structures were estimated using Heyd−Scuseria−Ernzerhof method. The band structures of pure and defect-induced CZASe materials are present in Figure 4. It is clearly seen that the highest occupied and lowest unoccupied energy bands of pure CZASe lie on the Γ-point, indicating a direct band gap of 2.08 eV. Here, the lowest energy conduction band appears to be isolated from the higher energy conduction bands. If the lower energy conduction band is fully unoccupied, then the optical excitation will be weak. For V_{Cu}, the top of the valence band does not show any variations because of the Cu vacant site when compared with the pure counterpart. It is noteworthy that the valence band edges of V_{Zn}, V_{Al}, Cu_{Zn}, and Cu_{Al} defects are up-shifted, while the low energy conduction band is down-shifted for Al_{Cu}. When compared with pure CZASe, the energy band gaps of V_{Zn}, V_{Al}, Cu_{Zn}, Al_{Cu}, Cu_{Al}, and Zn_{Al} are reduced, while the band gaps of V_{Cu}, Al_{Zn}, and Zn_{Cu} are increased.

https://doi.org/10.1021/acsomega.2c03223
ACS Omega 2022, 7, 31098−31105

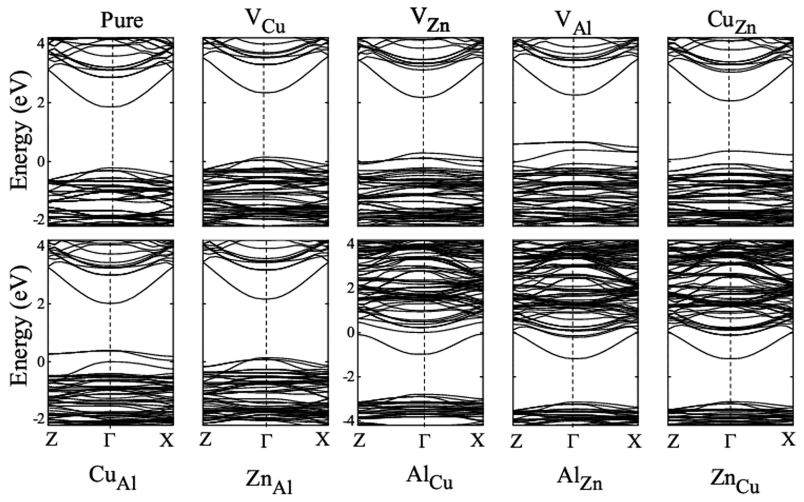

Figure 4. Calculated band structures of pure and defect-induced $CuZn_2AlSe_4$ materials.

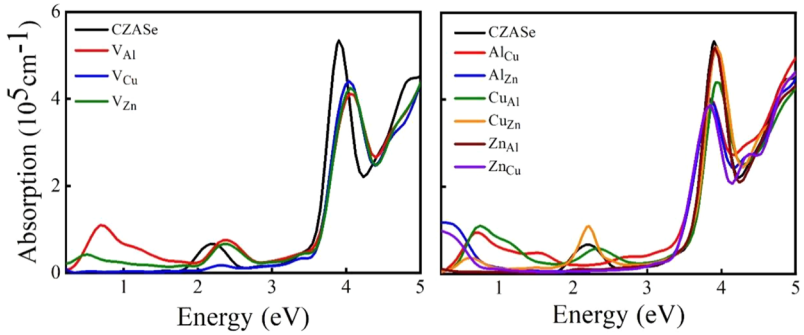

Figure 5. Calculated absorption spectrum of pure and defect-induced CZASe.

Overall, the maximum band gap corresponds to Al_{Zn} (2.74 eV), while the minimum one is for V_{Al} (1.56 eV). It should be noted that the defect induced states are determinantal to the performance of solar cells, as they act as recombination centers of photogenerated electron−hole pairs, thereby decreasing the effective optimal band gap and thus the open-circuit voltage (V_{oc}). Here, the effect of defects on CZASe induces energy band shifting and energy band narrowing or broadening. This tuning of band gap to achieve appropriate bandwidth can eventually improve the performance of the studied CZASe material.

To present a comprehensive analysis of electronic structure for all the model geometries with vacancies and defect, we examine the partial density of states as shown in Figure S2. The PDOS indicates that the valence band maximum (VBM) is mainly dominated by Zn and Se atoms, while the conduction band minimum (CBM) carries a mixture of Cu, Zn, Al, and Se atoms. The low energy CB around 2 eV is separated from other high energy CBs with a width of 0.7 eV. According to Luque and Marti,[33,34] the solar materials can achieve optimum power conversion efficiency when the valence to low energy CB gap is about 1.2 eV and the low to high energy CB gap is around 0.7 eV, which indicates the necessity of tuning the former gap, while the latter is of appropriate length. As discussed above, the introduction of vacancies and antisite defects in CZASe tunes the valence−low energy CB gap and thereby provides suitable bandwidth required for the model. This is clearly exemplified in the PDOS plot of V_{Zn} and V_{Al}, where the additional sharp peaks observed above the Fermi level in the spin-down channel of V_{Zn} and V_{Al} are due to the effect of defects in CZASe. Further, the spin down state above 0 eV for V_{Al} is more pronounced than V_{Zn}, Cu_{Zn}, and Cu_{Al}, which is in accord with the band structure, showing higher peaks for the corresponding defects. The energy bands of Al_{Zn} and Zn_{Cu} are shifted toward lower energy levels, and the effect of defects does not show any variations in the low energy CB and higher energy CB's gap.

4.3. Optical Properties. With the purpose of understanding the light absorption mechanism of defect-induced CZASe, the absorption spectra of CZASe in pure form and with vacancies and antisite defects are estimated using the HSE functional (see Figure 5). The absorption spectra of pure CZASe show the strongest absorption peak at around 3.9 eV, while the lowest band is observed at 2.2 eV. The introduction of vacancies expands the absorption spectrum and enhances the absorption intensity, thereby exhibiting blue shift in the spectrum from 2.2 eV for conventional CZASe to 2.3, 2.3, and 2.4 eV for V_{Al}, V_{Zn}, and V_{Cu}, respectively, while the intensities of the strong absorption peak are lowered and moved toward higher energies, indicating a blue shift in the absorption spectrum due to creation of vacancies.

More importantly, we could observe low energy excitations in the visible region of V_{Al} and V_{Zn} that can increase the solar absorbance of the material. In case of antisite defects, the band profile of the simulated spectrum shows marked variations when compared to that of pristine CZASe. For Cu_{Zn}, the intensity of the peak located around 2.2 eV is enhanced, while the strong intense peak at 3.9 eV is slightly lowered. In case of

https://doi.org/10.1021/acsomega.2c03223
ACS Omega 2022, 7, 31098−31105

Cu_{Al}, we could observe a blue shift in the absorption spectrum along with a decrease in the peak intensity. The Zn_{Al} antisite defect does not show any prominent enhancement in the visible light region, while new energy bands are created in the visible light region of Al_{Cu}, Cu_{Al}, and Cu_{Zn} defects.

4.4. Performance Parameters. For better understanding the performance of semiconducting CZASe material, we have calculated the current density and power conversion efficiency of pure and defect induced CZASe. Typically, the short-circuit current density (J_{sc}) is equivalent to the absorbed photon flux (J_{abs}) and can be predicted using the equation

$$J_{abs} = e\int_{E_g}^{\infty} A(E)J_{ph}(E)\,dE$$

where E_g, E, A, and J_{ph} represent the band gap, photon energy, absorbance, and incident photon flux, respectively, while the overlap between the solar spectrum and the absorbance upper limit of the theoretical energy conversion efficiency is

$$P = \frac{\int_0^{\lambda_{max}} W(\lambda)A(\lambda)C(\lambda)\,d\lambda}{\int_0^{\infty} W(\lambda)\,d\lambda}$$

Here, λ_{max} and λ represent the longest wavelength and the photon wavelength that can be absorbed by a material, respectively, while the solar spectral irradiance is denoted by $W(\lambda)$. A detailed description regarding the methodology can be found in our earlier report.[26]

The predicted band gap of pure CZASe is found to be 2.08 eV, and the corresponding current density and upper limit of the theoretical energy conversion efficiency are 9.9 mA/cm^2 and 8.13%, respectively. The calculated band gap, photocurrent density, and theoretical power conversion efficiency of pure and defect-induced CZASe are presented in Table 2. It can be clearly seen that the effect of vacancies and antisite defects show remarkable influence on both power conversion efficiency and current density. The Al vacant site (V_{Al}) shows an increment of 45% in current density when compared to pure CZASe, and the corresponding P is increased to 13.0%. It should be noted that the structure of Al vacant site has an appropriate band gap of 1.56 eV and thus produces maximum performance when compared to other defects. Similarly, the photocurrent densities of Cu_{Al} (16.8), Cu_{Zn} (16.6), Al_{Cu} (12.7), and V_{Zn} (13.1 mA/cm^2) are also increased when compared to its pure counterpart, and the corresponding P (%) is enhanced to 11.7%, 12.2%, 9.0%, and 10.0%, respectively. Interestingly, the valence band edges of these defects are shifted upward, indicating the decrease in the band gap. On the other hand, the Zn_{Al}, V_{Cu}, Zn_{Cu}, and Al_{Zn} suppress the current density from 9.9 mA/cm^2 to 5.8, 4.9, 3.4, and 3.4 mA/cm^2, and thus, the corresponding P is minimized to 4.2%, 3.82%, 2.71%, and 2.78%, respectively. These defect structures show larger band gaps (except Zn_{Al}) when compared to pure CZASe (see Figure 6). In addition, the P curves show sharp enhancement with increasing film thickness and the theoretical energy conversion efficiency approaches the saturation limit when the thickness of the film exceeds 1 μm. As shown in Figure 7a,b, the theoretical energy conversion efficiency (current density) for V_{Al}, Cu_{Zn}, Cu_{Al}, and Al_{Cu} are beyond 30% (30 mA/cm^2) when film thickness exceeds 1 μm, which is due to their band gap values being closer to the Shockley–Queisser limit, and thus, the corresponding systems have the ability to absorb large number of photons in the visible light spectrum.[28] Overall, V_{Al} and Cu_{Zn} defect systems with strong variations in the electronic band structure manifest the maximum theoretical energy conversion efficiency with respect to pure and other defected CZASe structures.

Table 2. Calculated Band Gap, Current Density (mA/cm^2), and Upper Limit of the Theoretical Energy Conversion Efficiency P (%) Considering 100 nm Film Thickness

structure	band gap (eV)	current density (mA/cm^2)	P (%)
pure	2.08	9.9	8.13
V_{Cu}	2.17	4.9	3.82
V_{Zn}	1.9	13.1	10.01
V_{Al}	1.56	18.0	13.0
Zn_{Cu}	2.71	3.4	2.76
Al_{Cu}	1.81	12.7	9.0
Cu_{Zn}	1.7	16.6	12.2
Al_{Zn}	2.74	3.4	2.78
Cu_{Al}	1.65	16.8	11.7
Zn_{Al}	2.0	5.8	4.2

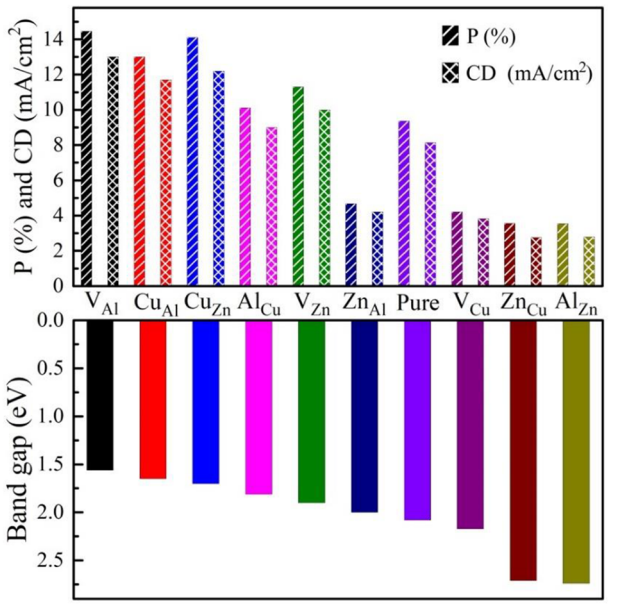

Figure 6. Graphical illustration of theoretical energy conversion efficiency P (%) and current density (mA/cm^2) plotted against the corresponding band gaps (eV).

5. CONCLUSION

In summary, we have proposed a novel quaternary semiconducting $CuZn_2AlSe_4$ chalcogenide through distant-atom mutation concept. The phonon dispersion spectrum confirms the dynamic stability of stannite CZASe material. Using first-principles HSE06 hybrid calculations, the vacancies and antisite defects as well as electronic and optical properties of CZASe were quantitatively analyzed. The narrow and complex region of CZASe indicates the importance of controlling chemical potential in developing good quality crystals. The antisite defect Cu_{Zn} has the lowest formation energy with a relatively deeper acceptor level than that of the Cu vacant site (V_{Cu}), which is mainly responsible for p-type conductivity. The electronic properties of vacancies and antisite defects show

https://doi.org/10.1021/acsomega.2c03223
ACS Omega 2022, 7, 31098−31105

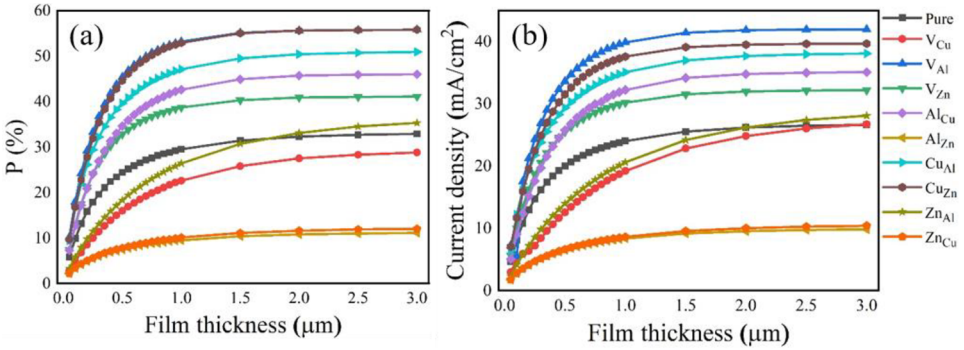

Figure 7. Computed (a) theoretical energy conversion efficiency and (b) current density of pure and defect-induced CZASe as functions of film thicknesses.

energy band shifting and energy band narrowing or broadening; in particular, the strong variations in the V_{Al} and Cu_{Zn} band structures manifest the maximum theoretical energy conversion efficiency with respect to pure and other defected CZASe structures. The introduction of low energy excitations in the visible light region of absorption spectrum for defect induced CZASe can eventually enhances the solar energy harvesting. Overall, the concept of cross-substitutions (cation mutations) can provide insights for modeling new solar light absorber materials with desirable photovoltaic applications.

■ ASSOCIATED CONTENT

Supporting Information

The Supporting Information is available free of charge at https://pubs.acs.org/doi/10.1021/acsomega.2c03223.

Secondary phases formation enthalpy, chemical potential, PDOS, and electrical performance parameters (PDF)

■ AUTHOR INFORMATION

Corresponding Author

Ranjit Thapa − *Department of Physics, SRM University-AP, Amaravati 522502 Andhra Pradesh, India;* orcid.org/0000-0002-9285-0525; Email: ranjit.t@srmap.edu.in

Author

M. V. Jyothirmai − *Department of Physics, SRM University-AP, Amaravati 522502 Andhra Pradesh, India; SRM Research Institute, SRM Institute of Science and Technology, Kattankulathur 603203 Tamil Nadu, India;* orcid.org/0000-0001-5024-0174

Complete contact information is available at: https://pubs.acs.org/10.1021/acsomega.2c03223

Author Contributions

R.T. conceived the project and designed the problem. M.V. J. performed the calculations and analyzed the data. R.T. and M.V.J. wrote the manuscript.

Notes

The authors declare no competing financial interest.

Data Availability. The data that supports the findings of this study are available within the article.

■ ACKNOWLEDGMENTS

M.V.J. and R.T. thank Ministry of New and Renewable Energy (MNRE), Government of India, for the financial support under the Grant No. 31/03/2014-15/PVSE-R&D. R.T. thanks Science and Engineering Research Board (SERB), India, for financial support (Grant No. CRG/2021/000620) and National Supercomputer Mission (NSM), India for financial support (Ref No.: DST/NSM/R&D_HPC_Applications/2021/19). The authors thank SRM Research Institute, SRM Institute of Science and Technology, for providing computational facilities.

■ REFERENCES

(1) Battaglia, C.; Cuevas, A.; De Wolf, S. High-Efficiency Crystalline Silicon Solar Cells: Status and Perspectives. *Energy Environ. Sci.* **2016**, *9* (5), 1552−1576.

(2) Qarony, W.; Hossain, M. I.; Hossain, M. K.; Uddin, M. J.; Haque, A.; Saad, A.R.; Tsang, Y. H. Efficient Amorphous Silicon Solar Cells: Characterization, Optimization, and Optical Loss Analysis. *Results Phys.* **2017**, *7*, 4287−4293.

(3) Liu, X.; Feng, Y.; Cui, H.; Liu, F.; Hao, X.; Conibeer, G.; Mitzi, D. B.; Green, M. The Current Status and Future Prospects of Kesterite Solar Cells: A Brief Review. *Prog. Photovoltaics Res. Appl.* **2016**, *24* (6), 879−898.

(4) Jiang, M.; Y, X. Cu_2ZnSnS_4 Thin Film Solar Cells: Present Status and Future Prospects. *Sol. Cells - Res. Appl. Perspect.* **2013**, DOI: 10.5772/50702.

(5) Hsu, W.-C.; Bob, B.; Yang, W.; Chung, C.-H.; Yang, Y. Reaction Pathways for the Formation of $Cu_2ZnSn(Se,S)_4$ Absorber Materials from Liquid-Phase Hydrazine-Based Precursor Inks. *Energy Environ. Sci.* **2012**, *5* (9), 8564−8571.

(6) Just, J.; Sutter-Fella, C. M.; Lützenkirchen-Hecht, D.; Frahm, R.; Schorr, S.; Unold, T. Secondary Phases and Their Influence on the Composition of the Kesterite Phase in CZTS and CZTSe Thin Films. *Phys. Chem. Chem. Phys.* **2016**, *18* (23), 15988−15994.

(7) Fan, F.-J.; Wu, L.; Gong, M.; Chen, S. Y.; Liu, G. Y.; Yao, H.-B.; Liang, H.-W.; Wang, Y.-X.; Yu, S.-H. Linearly Arranged Polytypic CZTSSe Nanocrystals. *Sci. Reports* **2012**, *2* (1), 1−6.

(8) Guijarro, N.; Guillén, E.; Lana-Villarreal, T.; Gómez, R. Quantum Dot-Sensitized Solar Cells Based on Directly Adsorbed Zinc Copper Indium Sulfide Colloids. *Phys. Chem. Chem. Phys.* **2014**, *16* (19), 9115−9122.

(9) Goodman, C. H. L. The Prediction of Semiconducting Properties in Inorganic Compounds. *J. Phys. Chem. Solids* **1958**, *6* (4), 305−314.

(10) Pamplin, B. R. A Systematic Method of Deriving New Semiconducting Compounds by Structural Analogy. *J. Phys. Chem. Solids* **1964**, *25* (7), 675−684.

(11) Ghosh, A.; Palchoudhury, S.; Thangavel, R.; Zhou, Z.; Naghibolashrafi, N.; Ramasamy, K.; Gupta, A. A New Family of Wurtzite-Phase Cu_2ZnAS_{4-x} and $CuZn_2AS_4$ (A = Al, Ga, In) Nanocrystals for Solar Energy Conversion Applications. *Chem. Commun.* **2016**, *52* (2), 264−267.

(12) Kevin, P.; Malik, M. A.; O'Brien, P. The AACVD of $Cu_2FeSn(S_xSe_{1-x})_4$: Potential Environmentally Benign Solar Cell Materials. *New J. Chem.* **2015**, *39* (9), 7046−7053.
(13) Ge, J.; Grice, C. R.; Yan, Y. Cu-Based Quaternary Chalcogenide Cu_2BaSnS_4 Thin Films Acting as Hole Transport Layers in Inverted Perovskite $CH_3NH_3PbI_3$ Solar Cells. *J. Mater. Chem. A* **2017**, *5* (6), 2920−2928.
(14) Liu, Q.; Cai, Z.; Han, D.; Chen, S. Natural Intermediate Band in I_2-II-IV-VI_4 Quaternary Chalcogenide Semiconductors. *Sci. Reports* **2018**, *8* (1), 1−8.
(15) Delgado, G. E.; Mora, A. J.; Grima-Gallardo, P.; Quintero, M. Crystal Structure of $CuFe_2InSe_4$ from X-Ray Powder Diffraction. *J. Alloys Compd.* **2008**, *454* (1−2), 306−309.
(16) Nagoya, A.; Asahi, R.; Wahl, R.; Kresse, G. Defect Formation and Phase Stability of Cu2ZnSnS4 Photovoltaic Material. *Phys. Rev. B* **2010**, *81* (11), 113202.
(17) Chaudhary, D. K.; Ghosh, A.; Thangavel, R.; Kumar, L. Bulk-Heterojunction Hybrid Solar Cells with Non-Toxic, Earth Abundant Stannite Phase $CuZn_2AlS_4$ Nanocrystals. *Thin Solid Films* **2018**, *649*, 202−209.
(18) Ghosh, A.; Thangavel, R.; Gupta, A. Chemical Synthesis, Characterization and Theoretical Investigations of Stannite Phase $CuZn_2AlS_4$ Nanocrystals. *New J. Chem.* **2016**, *40* (2), 1149−1154.
(19) Yalcin, B. G. Thermoelectric Properties of Stannite-Phase $CuZn_2AS_4$ (CZAS; A = Al, Ga and In) Nanocrystals for Solar Energy Conversion Applications. *Philos. Mag.* **2016**, *96* (21), 2280−2299.
(20) Shi, W.; Khabibullin, A. R.; Woods, L. M. Exploring Phase Stability and Properties of I-II_2-III-VI_4 Quaternary Chalcogenides. *Adv. Theory Simulations* **2020**, *3* (8), 2000041.
(21) Kresse, G.; Furthmüller, J. Efficiency of Ab-Initio Total Energy Calculations for Metals and Semiconductors Using a Plane-Wave Basis Set. *Comput. Mater. Sci.* **1996**, *6* (1), 15−50.
(22) Kresse, G.; Joubert, D. From Ultrasoft Pseudopotentials to the Projector Augmented-Wave Method. *Phys. Rev. B* **1999**, *59* (3), 1758.
(23) Perdew, J. P.; Burke, K.; Ernzerhof, M. Generalized Gradient Approximation Made Simple. *Phys. Rev. Lett.* **1996**, *77* (18), 3865.
(24) Heyd, J.; Scuseria, G. E.; Ernzerhof, M. Hybrid Functionals Based on a Screened Coulomb Potential. *J. Chem. Phys.* **2003**, *118* (18), 8207.
(25) Heyd, J.; Scuseria, G. E. Assessment and Validation of a Screened Coulomb Hybrid Density Functional. *J. Chem. Phys.* **2004**, *120* (16), 7274.
(26) Jyothirmai, M. V.; Saini, H.; Park, N.; Thapa, R. Screening of Suitable Cationic Dopants for Solar Absorber Material CZTS/Se: A First Principles Study. *Sci. Reports* **2019**, *9* (1), 1−12.
(27) Togo, A.; Tanaka, I. First Principles Phonon Calculations in Materials Science. *Scr. Mater.* **2015**, *108*, 1−5.
(28) Shockley, W.; Queisser, H. J. Detailed Balance Limit of Efficiency of P-n Junction Solar Cells. *J. Appl. Phys.* **1961**, *32* (3), 510.
(29) Gloeckler, M.; Sites, J. R. Band-Gap Grading in $Cu(In,Ga)Se_2$ Solar Cells. *J. Phys. Chem. Solids* **2005**, *66* (11), 1891−1894.
(30) Jackson, A. J.; Walsh, A. Ab Initio Thermodynamic Model of Cu_2ZnSnS_4. *J. Mater. Chem. A* **2014**, *2* (21), 7829−7836.
(31) Chen, S.; Gong, X. G.; Walsh, A.; Wei, S.-H. Defect Physics of the Kesterite Thin-Film Solar Cell Absorber Cu_2ZnSnS_4. *Appl. Phys. Lett.* **2010**, *96* (2), 021902.
(32) Scragg, J. J.; Dale, P. J.; Peter, L. M.; Zoppi, G.; Forbes, I. New Routes to Sustainable Photovoltaics: Evaluation of Cu_2ZnSnS_4 as an Alternative Absorber Material. *Phys. status solidi* **2008**, *245* (9), 1772−1778.
(33) Luque, A.; Martí, A.; Stanley, C. Understanding Intermediate-Band Solar Cells. *Nat. Photonics* **2012**, *6* (3), 146−152.
(34) Luque, A.; Martí, A. Increasing the Efficiency of Ideal Solar Cells by Photon Induced Transitions at Intermediate Levels. *Phys. Rev. Lett.* **1997**, *78* (26), 5014.

https://doi.org/10.1021/acsomega.2c03223
ACS Omega 2022, 7, 31098−31105